TRANSPHORM

Transport related Air Pollution and Health impacts – Integrated Methodologies for Assessing Particulate Matter

Collaborative project, Large-scale Integrating Project

SEVENTH FRAMEWORK PROGRAMME

ENV.2009.1.2.2.1 Transport related air pollution and health impacts

Deliverable D1.3.3
Report

Non-anthropogenic emission evaluation

Due date of deliverable: project month 18

Actual submission date: project month 18

Start date of project: 1 January 2010 Duration:	48 months
Organisation name of lead contractor for this deliverable:	FMI
Scientist responsible for this deliverable:	Dr. M.Sofiev

Contents

Objectives

The task 1.3.3 provides complementary information on non-anthropogenic emissions, which is needed for efficient mass closure and model-measurement comparison. These include: (i) biogenic organic compounds, (ii) biomass burning smoke, (iii) wind-blown dust and (iv) sea salt. Depending on the regions and specific episodes, one or more of these sources can be dominant. Several inventories exist for each of these sources but extreme temporal variability of these sources limit the value of these inventories. Therefore, this task will concentrate on actual modelling of these emission fluxes and resulting concentrations of the released pollutants. The SILAM modelling system contains dedicated modules for each of these compounds, which generate the emission fluxes using actual meteorological conditions and remote-sensing observations wherever appropriate. The dispersion block of the system then produces the dispersion products, such as concentrations, optical properties of the plumes, and depositions. Both emission and dispersion products are available for the TRANSFORM partners.

This delivery report for the non-anthropogenic PM emission evaluation concentrates on the wild-land fire emission inventory and also presents the modules of the SILAM system responsible for the desert dust and sea salt wind-driven emission. These inventories and modules have been developed / refined within the scope of TRANSFORM WP 1.3.

Since SILAM is a multi-scale model and can be run both globally and regionally, the report covers both global and regional scales. The global fire inventory and corresponding modules and outcome of the simulations comprise the contribution to the Delivery 1.3.4.

Global and European emission inventory for wild-land fires.

The global and European fire emission inventory has been compiled using the Fire Assimilation System (FAS) of FMI (Sofiev *et al*, 2009). It uses two remotely sensed wild-land fire characteristics: 4-μm Brightness Temperature Anomaly (TA) and Fire Radiative Power (FRP) - for the needs of emission estimation from wild-land fires. Two treatments of the TA and FRP data comprise the methodology that is applied for evaluating the emission fluxes from the MODIS level 2 fire products.

The FAS does not contain a complicated analysis of vegetation state, fuel load, burning efficiency and related factors, which are uncertain but inevitably involved in approaches based on burnt-area scars or similar products. The core of the current methodology is based on the fire intensity expressed either via TA or FRP values, which are converted into emission of atmospheric pollutants via empirical emission factors derived from the analysis of several fire episodes. These calibration episodes were characterised by: (i) well-identified FRP and TA values, and (ii) available independent observations of aerosol concentrations and optical thickness for the regions where fire smoke was dominant in comparison with contributions of other pollution sources. The emission factors were determined separately for the forested and grassland areas, whereas the intermediate scaling is used in case of mixed-type land use. That made them applicable also beyond the episodes, for which they were derived, using the land-use as the surrogate for the extrapolation.

Despite significant difference between the TA and FRP products, an accurate non-linear fitting between the approaches was found and used for gap-filling (Figure 1). The fit is comparatively weak only for small fires where the accuracy of both products is low. The re-analysis and forecasting applications of the Fire Assimilation System (FAS) showed that both TA and FRP products are suitable for evaluation of the emission fluxes from the wild-land fires.

The evaluation of the emission system is based on the concentrations of aerosols predicted by the regional dispersion modelling system SILAM using the FAS emission fluxes. In the considered cases, the model predictions appear within a factor of 2-3 from observations.

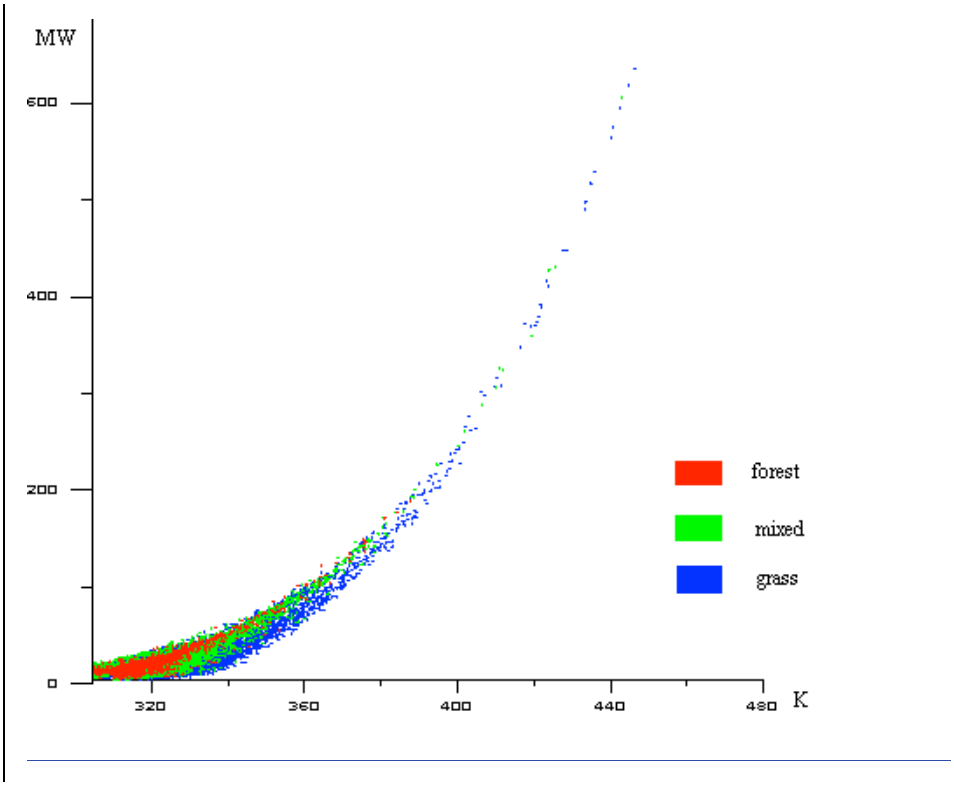

Figure 1. A relation between the fire intensity indicators. The brightness temperature, [K] from 21-st band of MODIS (horizontal axis) is related to FRP for the same fire pixel from MOD14 fire product [MW per pixel area] (vertical axis). Colours of the dots correspond to the land cover types (red – forest, green - mixed forest and grass, blue – grass only).

Global and European fire emission databases

Both global and European databases cover the period from 2000 till 2011 with temporal resolution of 1 day and spatial resolution of 0.5 degree for global and 5km for European datasets. Two examples of the fire emission are shown in Figure 2 for global (sum over July-August 2010) and in Figure 3 for Europe (sum over 2006).

The temporal variation of the emission fluxes are shown in Figure 4. Note that during the first two years only Terra satellite was on duty, so that the coverage of the retrievals was not sufficient for reliable emission retrieval. In particular, the observations over Africa were taking place in the morning and evening, i.e. when the fires were either not yet at full power or already partly extinguished. The present system formulations seem to be sensitive to this issue: the diurnal variation is too conservative. The next-stage work will be to improve the database in this regard.

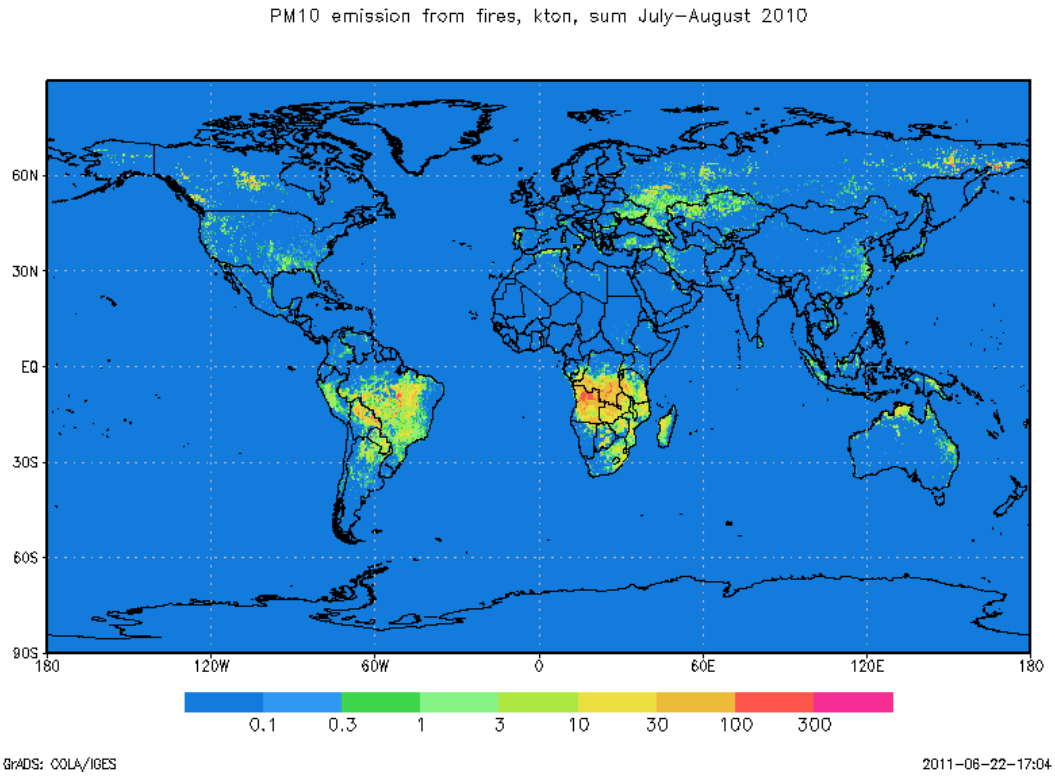

Figure 2. Sum of the PM10 emission from wild-land fires, sum July-August 2010, ktons per grid cell.

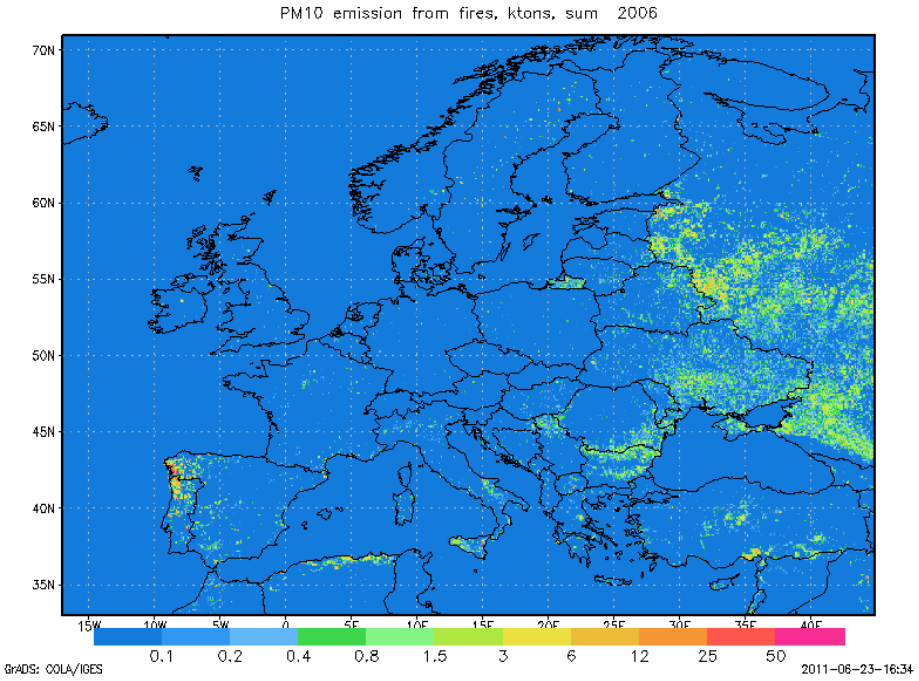

Figure 3. Sum of PM10 emission from wild-land fires, sum 2006, ktons per grid cell.

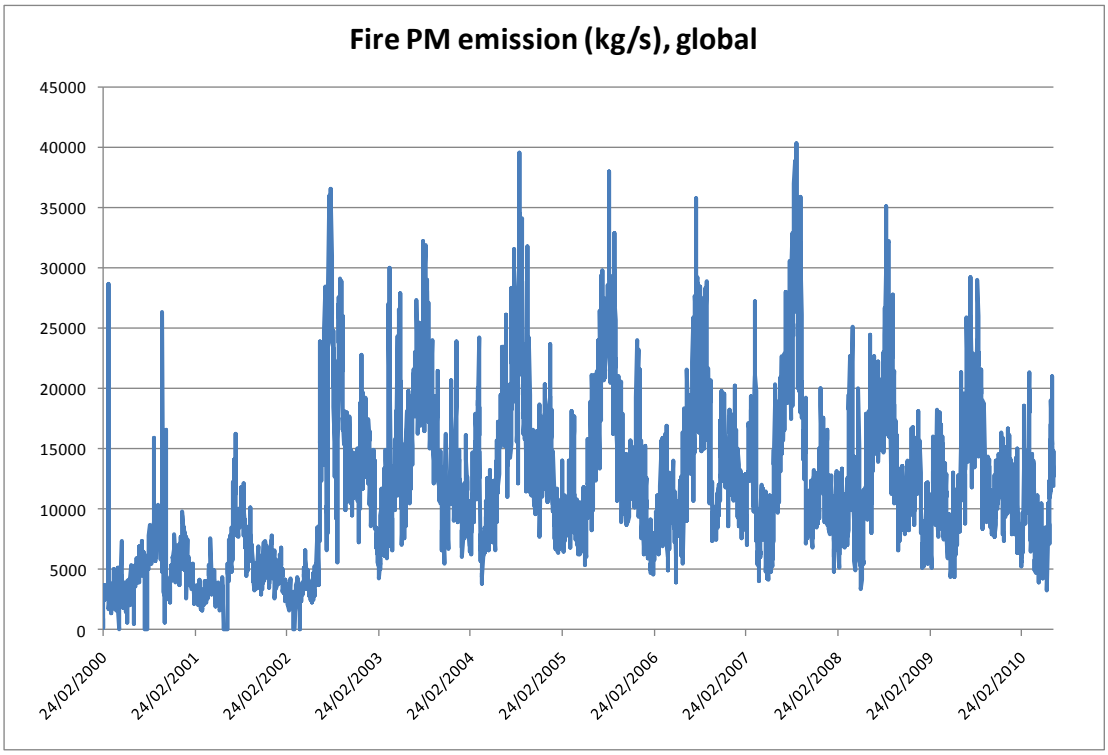

Figure 4. Temporal evolution of the global emission from wild-land fires. During the first two years only MODIS onboard of Terra was available.

Sea salt emission module in the SILAM system

The SSA production term of the SILAM modelling system (Sofiev et al, submitted) is based on the parameterisation of Monahan *et al.* and on experimental data from Mårtensson *et al.*, and Clarke *et al*. The observational data were used to extend the Monahan *et al.* SSA emission flux to particles as small as 10 nm (dry particle diameter D_P) and to account for water temperature and salinity. The result is an analytical formulation describing the SSA production fluxes for particles with D_p between 10 nm and 10 μm. Present applications of the model for the evaluation purposes include the computation of sea salt distributions over the North Atlantic and Western Europe for the years 2000, 2003, 2007, 2009 and 2010, as well as globally for 2001 and 2008. The computed annual global production of SSA is between 6700 and 7400 Tg/year. Evaluation of the SSA spectrum in North-East Atlantic showed good agreement wit the NEAT cruise campaigns. Comparison of the SILAM near-surface SSA concentrations and its wet deposition with the in-situ EMEP observations showed good agreement for summer periods while in winter time the model tends to under-estimate the wet deposition by a factor of ~3. The underestimation is attributed to the coarse fraction (D_p>10μm) and the spume production mechanism, which were excluded from the analysis, to the wet deposition parameterization in SILAM and to the low bias in the input precipitation data. The predicted vertically integrated aerosol optical depth (AOD) showed a close match with satellite observations over SSA-dominated areas.

An example of the global SSA-induced AOD and its comparison with MODIS retrievals is shown in Figure 5.

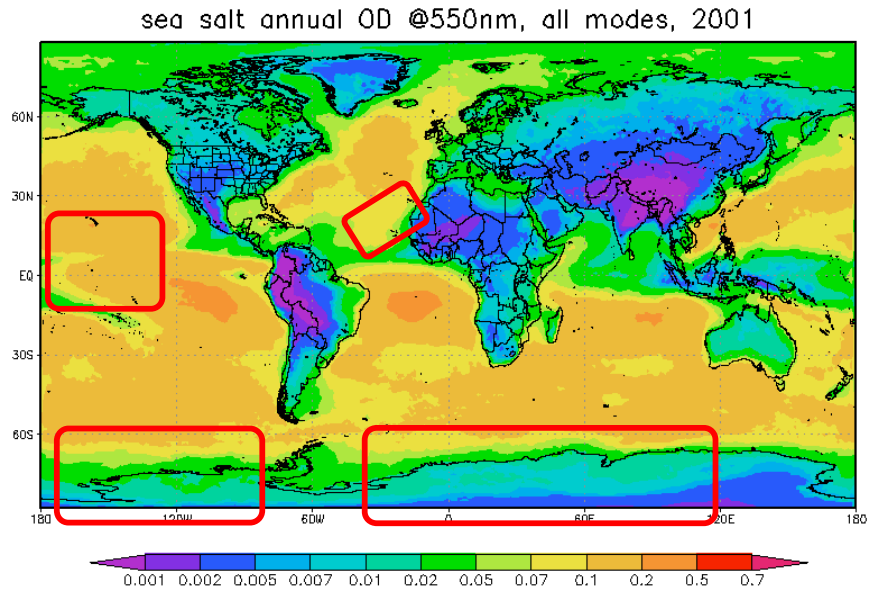

a).

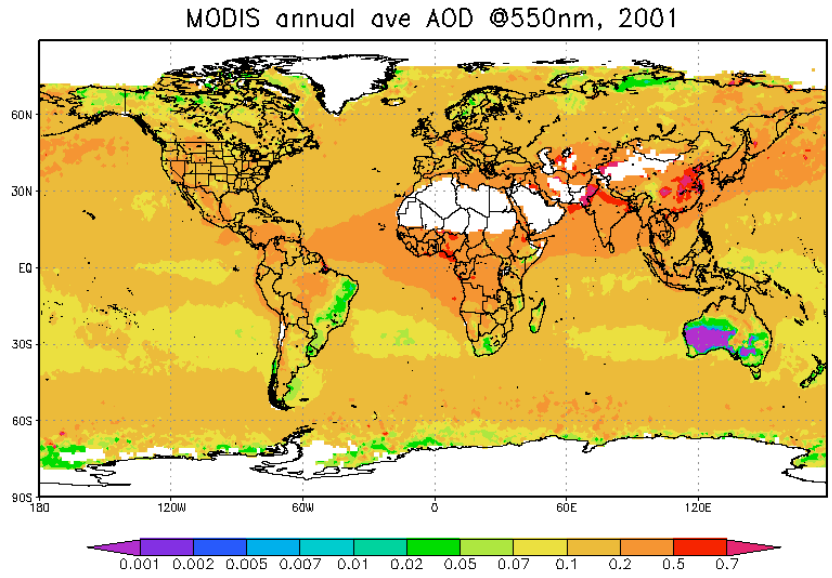

b).

Figure 5. Mean AOD for 2001: a) SILAM predicted AOD due to sea salt only, co-located with MODIS data; b) AOD due to all aerosol types observed by MODIS (http://disc.sci.gsfc.nasa.gov/giovanni). Red rectangles show the SSA-dominated areas where AOD from MODIS can be compared with SSA-only SILAM AOD.

Model for desert dust emission

The sources of natural wind-blown dust include: (i) dust eroded and uplifted by wind from arid areas and deserts, agricultural lands and bare lands. In the case of regional simulations, dust sources outside the model domain are incorporated via the boundary conditions.

Dust entrained into the atmosphere consists of the clay-sized ($D_p < 2.5\ \mu m$) and the silt-sized ($2.5 < D_p < 60\ \mu m$) particles. However, they are not directly mobilized by the wind since the cohesive forces (capillary and electrostatic) bind these particles into the soil structures. Currently, the mechanism releasing these particles is widely accepted to be the bombardment by coarser particles involved in the saltation process (the sandblasting mechanism – Iversen and White, 1982; Shao *et al*., 1996; Alfaro and Gomes, 2001; Grini *et al.*, 2002). Sandblasting refers to the disaggregation and ejection of clay and silt particles by saltating sand-sized particles ($D_p > 60\ \mu m$).

The potentially important alternative mechanism involves thermal destruction of the binding forces in the upper soil layer followed by either mechanical (by wind stress) or thermophoretic mechanism of the initial uplift of both clay- and silt-sized aerosols. Some indications of this mechanism were observed in a series of field campaigns in Caspian and Aral deserts (Gletzer *et al.,* 2009, 2010). However, there is no quantitative description of the related processes and the approach does not seem to be fully developed, therefore this mechanism is left out of the current parameterization.

The current parameterization of the saltation mechanism generally follows the work of Marticorena and Bergametti (1995, hereinafter referred to as MB95) and Zender (2003, hereinafter referred to as Z03).

The most important parameter of the saltation process is the minimum surface stress required to involve the coarse particles into horizontal movement. It is expressed as the threshold friction velocity u_t^*, which, following Iversen and White (1982), depends on the critical Reynolds number of the saltating particles:

(1) $$u_t^* = f(\mathrm{Re}_c) = f(u_t^* D_p / \nu),$$

where ν is the kinematic air viscosity and the function *f* is established empirically.

Since the function *f* is non-linear of Re_c, which itself contains u_t^*, the equation (1) has to be solved numerically. It is neither practical in large-scale simulations due to high costs nor justified due to high uncertainty of all input parameters and working hypotheses.

Analysis of the solution for the relevant ranges of air and particle density, as well as the particle diameter, shows that there is an "optimal" diameter D_{salt_opt}, which is a function of ρ_{part} only. Particles of this size are first to be involved into saltation, i.e. at the lowest u^*. Its variation is quite weak and for the density varying from 2000 kg m^{-3} to 3000 kg m^{-3}, the variation range of the optimal diameter is about 15%. At the same time, $\rho_{part} D_{part}^2$ for the same range of density varies by 6%. So, let's say that this is constant and its value is $1.41 \cdot 10^{-5}$ kg m^{-1}. Interestingly, if the power at the D_{part} is about 2.4 then the variation is way below 1%. Therefore, one can simply assume that the "optimal" size of particles that are first involved in saltation follows from the equation:

(2)
$$D_{salt\_opt} = 0.0018 \rho_{part}^{0.4}$$

For critical friction velocity (the most sensitive parameter) the dependences are shown in Figure 6. The dimensions are evidently separated, so that it is possible to write the u^* dependence on air and particle density in the following form:

(3)
$$u^*_{crit} = 0.063 \cdot \left(\frac{\rho_{part}}{\rho_0} \right)^{0.31} \left(\frac{\rho_{air}}{\rho_0} \right)^{-0.46}$$

where $\rho_0 = 1\ kg\ m^{-3}$.

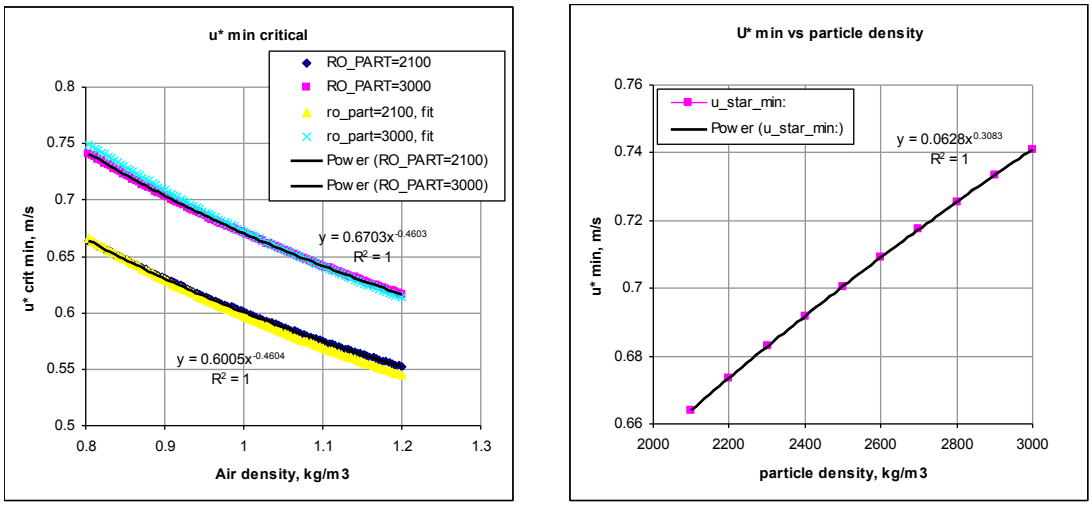

Figure 6. Dependence of minimal critical friction velocity on air and particle density (left) and on particle density (right)

Due to high uncertainty of all the components of the model, one can argue that a simpler and, possibly, more intuitively understandable formulation would be:

(4)
$$u^*_{crit} = 0.0466 \cdot \left(\frac{\rho_{part}}{\rho_0} \right)^{1/3} \left(\frac{\rho_{air}}{\rho_0} \right)^{-1/2}$$

Its difference from the original formulations (3) does not exceed 2% for the relevant ranges of the air and particle densities (Figure 6).

Following Z03 we account for two processes additionally affecting the u_t^*: partitioning the drag between the erodible and non-erodible elements of the surface and the soil humidity-driven reduction of the saltation efficiency.

The drag partitioning is expressed by MB95 via a bulky relation involving the extremely poorly known parameters, such as the roughness lengths for the erodible and non-erodible parts of the landscape. However, a quick check shows that this relation varies from about 0.9 up to about 2 for all imaginable surfaces of interest. For the most-typical values, it is about 1.3, which is used further as a scaling factor for u_t^*.

The humidity correction is also poorly identified. Several empirical dependencies have been elaborated (Belly, 1964; Pye, 1987; Gillette, 1988; Selah and Fryrear, 1995; Shao et al., 1996; Fecan et al., 1999, etc) but nearly the only message these parameterizations agree on is that when the gravimetric fraction of water in soil approaches 0.5 kg kg^{-1} the erosion becomes impossible for any feasible wind stress. From the other side, the meteorological models and observations (e.g. remote sensing) tend to provide non-zero amount of water everywhere including even the driest deserts (Zender, 2002). This has to be taken as uncertainty of the parameter, which is sometimes reflected via threshold water content that depends on a fraction of clay in the soil. In absence of other justification, we used a simple correction function that accounts for the above physical requirements:

(5)
$$f_w = \begin{cases} \dfrac{1}{1 - 4 * w^2}, & w < 0.5 \\ \infty, & w \geq 0.5 \end{cases}$$

It is smooth, differs from unity by less than 1% for w up to $0.05\ kg\ kg^{-1}$, and approaches infinity when $w \rightarrow 0.5\ kg\ kg^{-1}$.

Once the erosion starts, the Owen (1964) effect increases the u^* as a result of a positive feedback of saltation. Therefore, the wind speed needed to start the saltiation is higher than the one needed to support it once started. For instance, the wind gust can be the starting trigger with the mean wind still lower than the threshold. To reflect this phenomenon, we introduced the smoothly increasing saltation intensity growing with u^*, which is non-zero starting from the moment when the mean speed plus gust fluctuations are equal to the threshold.

The saltation mass flux of loose soil particles follows White (1979):

(6)
$$Q_s = \frac{C\rho_{air}}{g} u_*^3 \left(1 - \frac{u_t^*}{u_*}\right)\left(1 + \frac{u_t^*}{u_*}\right)^2$$

where Q_s is the horizontal mass flux of soil particles (kg $m^{-1}s^{-1}$), ρ_{air} is the air density, g is the gravitational acceleration and C=2.6 is the empirical constant.

The efficiency of sandblasting mechanism depends on the amount of clay ready to be injected in the air. With high care, one can try the MB95 connection:

(7)
$$\alpha = 100 \cdot 10^{13.4 M_{clay} - 6}$$

where M_{clay} is the mass fraction of the clay particles in the soil. Z03 warns about the hard limit for it as 0.2. Should it be given free run, the Asian deserts start producing much too much dust.

The total vertical flux of dust particles released by sandblasting mechanism is then simply:

(8)
$$F = A_s K \alpha Q_s$$

Where F is the vertical mass flux of dust [kg m^{-2} s^{-1}], A_s is the area fraction of erodible soil in the grid cell, K is the coefficient accounting for soil erodibility (availability of loose soil aggregates), α is the sandblasting efficiency.

Based on the experimental results in Gomes (2003), EMEP suggested the following empirical values: $\alpha = 2.0 \cdot 10^{-5}$, $1.5 \cdot 10^{-5}$, $1.0 \cdot 10^{-5}$ and $0.8 \cdot 10^{-5}$ m^{-1} and K = 0.5, 0.1, 0.05 and 0.01 for Northern Sahara, other desert areas in Europe, Mediterranean, and temporal agricultural lands respectively.

The sandblasting mechanism implies the static aerosol spectre in the air: it is fully defined by the soil type and can be parameterised directly from the observations. As an option, the data from B.Weinzierl (2007) dissertation can be used where 4 log-normal modes were fit for the parameterization.

	Nmode 1	CMDmode	GSDmode	Nmode 2	CMDmode	GSDmode	Nmode 3	CMDmode	GSDmode	Nmode 4	CMDmode	GSDmode
average	925.28	0.07	1.94	72.97	0.36	1.59	22.22	0.98	2.05	1.18	5.66	1.72
stddev	642.42	0.01	0.26	61.52	0.19	0.12	15.18	0.35	0.12	1.10	1.48	0.18

CMD = count mean diameter, GSD = geometric standard deviation

This static-spectrum approach is in certain contrast with some parameterizations, which connect the flux for the specific size bin with the wind speed. However, in absence of strong evidence in favour of the more complicated description, the static-spectrum description seems to be a plausible compromise.

References

Alfaro, S. C., Gomes, L., (2001) Modeling mineral aerosol production by wind erosion: Emission intensities and aerosol size distributions in source areas, J. Geophys. Res., 106, 18,075– 18,084

Belly, P. Y., (1964) Sand movement by wind, Tech. Memo. 1, U.S. Army Coastal Eng. Res. Cent., Vicksburg, Miss.

Fecan, F., Marticorena,B., Bergametti,G. (1999) Parametrization of the increase of the aeolian erosion threshold wind friction velocity due to soil moisture for arid and semi-arid areas, Ann. Geophys., 17, 149 – 157

Gillette, D. A. (1988) Threshold friction velocities for dust production for agricultural soils, J. Geophys. Res., 93, 12,645– 12,662

Gledzer, E.B., Granberg, I.G., Chkhetiani, O.G. (2009) Convective Aerosol Fluxes near the Ground Surface, ISSN 1028-334X, Doklady Earth Sciences, 2009, Vol. 426, No. 4, pp. 652–657. Pleiades Publishing, Ltd.

Gledzer, E.B., Granberg, I.G., Chkhetiani, O.G. (2010) Air Dynamics near the Soil Surface and Convective Emission of Aerosol ISSN 0001_4338, Izvestiya, Atmospheric and Oceanic Physics, 2010, Vol. 46, No. 1, pp. 29–40. Pleiades Publishing, Ltd.

Grini, A., Zender,C.S., Colarco, P. (2002) Saltation sandblasting behaviour during mineral dust aerosol production, Geophys. Res. Lett., 29(18), 1868, doi:10.1029/2002GL015248

Iversen, J. D., and B. R. White (1982) Saltation threshold on Earth, Mars, and Venus, Sedimentology, 29, 111– 119

Marticorena, B., Bergametti, G., (1995) Modeling the atmospheric dust cycle: 1. Design of a soil-derived dust emission scheme, J. Geophys. Res., 100, 16,415–16,430

Owen, P. R. (1964) Saltation of uniform grains in air, J. Fluid Mech., 20, 225–242

Selah, A., Fryrear,D.W. (1995)Threshold wind velocities of wet soils as affected by wind blown sand, Soil Sci., 160, 304–309

Shao, Y., Raupach, M.R., Leys, J.F. (1996) A model for predicting Aeolian sand drift and dust entrainment on scales from paddock to region, Aust. J. Soil Res., 34, 309– 342

Sofiev,M., Vankevich,R., Lotjonen,M., Prank,M., Petukhov,V., Ermakova,T., J.Koskinen, Kukkonen,J. (2009). An operational system for the assimilation of satellite information on wild-land fires for the needs of air quality modelling and forecasting. Atmos. Chem. Phys., 9, 6833-6847, http://www.atmos-chem-phys.net/9/6833/2009/acp-9-6833-2009.html.

Weinzierl, B.B. (2007) Radiatively-driven processes in forest fire and desert dust plumes Dissertation an der Fakultät für Physik der Ludwig-Maximilians-Universität, München.

White, B. R., (1979) Soil transport by winds on Mars, J. Geophys. Res., 84, 4643– 4651

Zender, C.S, Bian, H., Newman, D. (2003) Mineral Dust Entrainment and Deposition (DEAD) model: Description and 1990s dust climatology. JGR, 108, NO. D14, 4416, doi:10.1029/2002JD002775